



## USING GA-BASED INTELLIGENT CONTROL MEANS TO ENHANCE HUMAN-MACHINE INTERFACES<sup>1</sup>

**D. W. REPPERGER**

*Air Force Research Laboratory  
AFRL/HECP  
WPAFB, Ohio, USA*

*and*

**LING ROTHROCK**

*Department of Industrial and Manufacturing Engineering,  
The Pennsylvania State University  
University Park, PA 16802 US*

**ABSTRACT**—A GA (genetic algorithm) search procedure was employed to explore a best set of sensory feedback parameters in designing a human-machine interface for improved performance. The optimization concerned two objective functions of interest, which incorporated tradeoffs between speed and accuracy in tracking. A Pareto-optimal front was calculated involving the two cost functions selected. This approach differs from the traditional minimum of a non-convex cost function (scalar) describing the desired closed loop performance. Also, this methodology used a parsimonious experimental design method. By making a few runs with a limited number of subjects, a response model was first developed. This model was then simulated and a complex vector response surface was generated by the performance variables of interest. The GA search procedure was then used to locate the minimum of this response surface. Finally, in a post hoc experimental study to confirm that the selected design parameters were the best from the class selected, seven human subjects were evaluated at the most favorable experimental design parameters and compared to alternative conditions.

**Key Words:** man-machine interface, multiobjective evolutionary algorithms

### 1. INTRODUCTION

As human interact with machines, performance and other task attributes produce nonlinear interactions characterized via complex response surfaces that need to be explored to find the most favorable operating conditions. Humans have numerous and multifaceted objectives as they tend to optimize their performance in difficult task scenarios. For multiple objective functions, genetic algorithms (GAs) provide a powerful platform to explore these complex surfaces using a Pareto-optimal front. In addition, vector objective function formulations can be created to exemplify these complex interactions. The term “Pareto-optimal” refers to a curve comprising two or more cost functions that are to be optimized. Along this curve, both cost functions are minimized or maximized. The solutions are called “non-dominant” along the curve of the Pareto-optimal front if no solution is any better than the other. This means both cost functions are equally optimized along this curve. The solutions would be “dominant” if one cost function received a greater benefit as compared to another (competing) cost function. The objective functions described herein relate two conflicting output goals of the human operator (accuracy versus speed), which naturally compete with each other. The tracking task, itself, also has competing interactions (target tracking and disturbance rejection), which is typical of an operationally relevant scenario.

---

<sup>1</sup> Supported, in part, by a grant from the Office of the Chief Scientist, Human Effectiveness Directorate, AFRL/HE with title, “Applying Genetic Algorithms to the Design of Human Interface Systems,” 2001.

The GA methodology employed, herein, includes an analysis of the key parameters through a MATLAB™ model simulation. An empirical pilot study was first conducted using human subjects to help develop the initial model and a MATLAB™ imitation of the process. The computer simulation (MATLAB/SIMULINK™) was then run  $65,536 = 2^{16}$  times to predict the appropriate performance metrics. The GA method then searched the computer generated response surface for the enhanced design parameters. Then using the enhanced parameters in a post hoc evaluation, additional human data were then collected to validate (experimentally) that the best design conditions selected demonstrated the desired efficacy as compared to alternative choices.

In the intelligent control literature, there is much interest in studying how humans interact with complex systems. In [1] Fuzzy control methods were used to discern patterns of response behavior, which could then lead to an adaptation of a controller for neurologically, challenged patients. In [2], supervisory control systems had their automation level adjusted using fuzzy and neural networks. In [3], an intelligent control system was designed, which was robust to noisy disturbances. In [4] the control system would mimic, in an intelligent manner, the behavior of human operators and performed well, as compared to manual control. Adaptive and fuzzy fusion techniques are also very popular [5]. The applications of genetic algorithms are deemed very pervasive in the intelligent control literature. For example, in helping to tune a fuzzy logic controller [6], a power system was shown to have improved transient stability. In conjunction with neural networks, learning algorithms can be enhanced with the help of evolutionary algorithms [7,8]. Additional applications include feature extraction and pattern recognition where optimization methods present a framework to enable competent decisions [9]. One aspect of optimization involves the calculation of the objective functions as a vector process, rather than dealing with a single scalar cost function. The Pareto-optimal front provides a platform to examine the class of optimal solutions and to evaluate implicit tradeoffs between the respective objective functions within the region of optimality. This adds new information in understanding the underlying physical process.

The next section will introduce the concept of a Pareto-optimal front. In optimization studies, this describes when an optimal solution may exist over an interval or range of values, rather than at a single point. Since this is an interval of solutions, these solutions are termed **nondominant**, with respect to a certain performance criterion (non are better than another). What is new and useful in this procedure is that it is possible to probe deeper into the problem to better understand why the optimization function behaves in this manner over this interval. This gives new physical insights into what is going on.

## 2. PARETO-OPTIMAL FRONTS FOR MULTI OBJECTIVE MINIMIZATION

Pareto-optimal fronts provide an interesting mechanism to glean out how certain objective functions (subsets of the original objective function) may trade off, one against the other, during an optimization procedure. We first present an example to illustrate how this technique provides new information on the tradeoff of key variables within a dynamical process.

**Example 1:** Find an optimal point (or set) to minimize an objective function  $J_1(x)$  where:

$$\min J_1(x) = J_2(x) + \alpha J_3(x) \quad (\alpha = 1) \quad (1)$$

where  $J_2(x) = x^2 \quad (2)$

$$J_3(x) = (x-2)^2 \quad (3)$$

The issue here is to minimize  $(J_2 + \alpha J_3)$ . With reference to Figure 1, the curves of  $J_2$  and  $J_3$  are plotted versus  $x$ . It is noted that three intervals are of interest in this example which can be described below. The Pareto-Optimal Front occurs when  $x \in [0, 2]$ .

Please note the following three intervals of interest:

- (1) For  $x < 0$ ,  $J_2$  increases,  $J_3$  increases and  $J_1$  increases.
- (2) For  $x > 2$ ,  $J_2$  increases,  $J_3$  increases and  $J_1$  increases.

However:

- (3) For  $0 \leq x \leq 2$ ,  $J_2$  increases,  $J_3$  decreases and  $J_1$  decreases to  $x = 1$  and then increases. Thus only in the region  $0 \leq x \leq 2$ , is there a tradeoff between  $J_2$  and  $J_3$  to achieve the common goal of minimizing  $J_1$ . The Pareto-optimal front is the region where the constituent cost functions  $J_2$  and  $J_3$  interact with one another

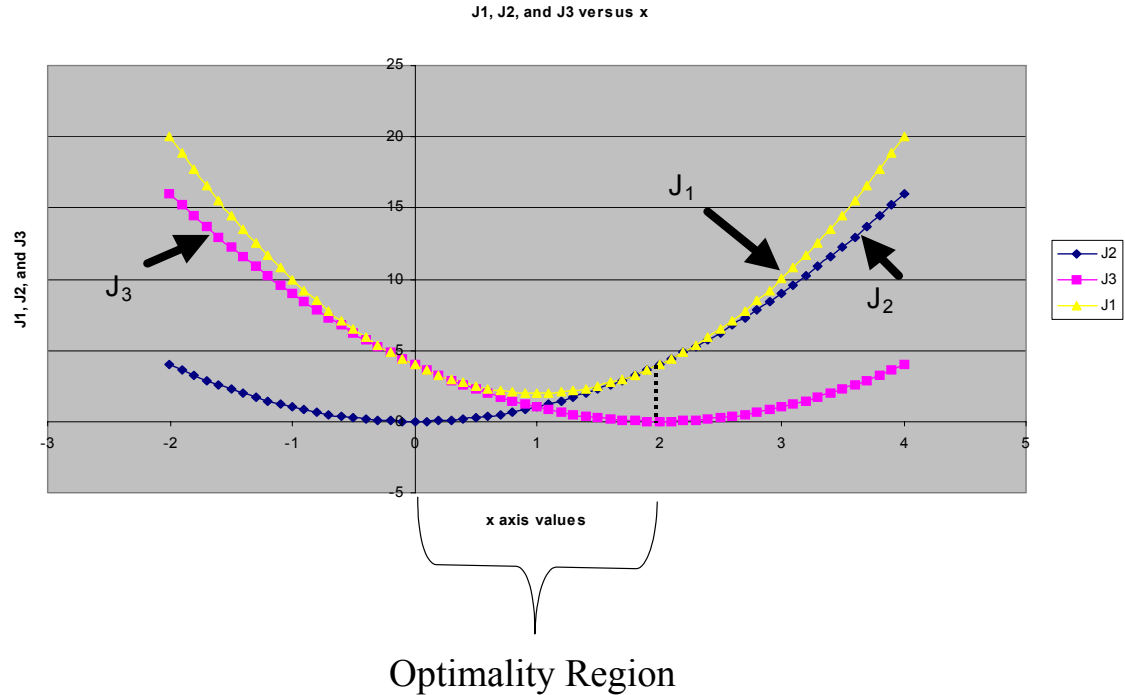


**Figure 1.**  $J_1$ ,  $J_2$  and  $J_3$  versus  $x$  for Example 1.

having the common goal of minimizing the overall cost function  $J_1$ . The interaction is conflicting (as  $J_2$  increases,  $J_1$  decreases, and conversely).

In this interval ( $0 \leq x \leq 2$ ), if an attempt is made to minimize  $J_3$ ,  $J_2$  will correspondingly increase. Thus a tradeoff occurs and the point of optimality would change if  $J_2$  and  $J_3$  were not equally weighted, ( $\alpha \neq 1$ ) as indicated in equation (1). This is termed the interval of nondominant solutions. The optimal solution for example 1 (equal weightings on  $J_2$  and  $J_3$ ) is, of course, the point  $x = 1$ , which is easily determined when  $\alpha = 1$ . This example can now be viewed in a more general context (for all  $\alpha \neq 1$ ).

**Example 2:** Find the optimal point (or set) to minimize  $J_2$  and  $J_3$ , where  $J_2$  is specified in equation (2) and  $J_3$  is specified in equation (3).

Referring back to Figure 1, the solution still occurs on the interval  $x \in [0, 2]$  because a tradeoff exists between the two objective functions  $J_2$  and  $J_3$  in this interval. Figure 2 illustrates a plot of  $J_3$  versus  $J_2$  for  $x \in [0, 2]$ . What is now very interesting is that Figure 2 portrays how this tradeoff occurs over the optimal interval of interest. The condition ( $\alpha = 1$ ) can be replaced by a tangent to this curve ( $J_2 + J_3 = \text{constant}$  or having equal weightings) which would indicate that the minimum solution of example 1 occurs at the point  $x = 1$  in Figure 2. Thus, example 1 is a subset of example 2. The curved surface in Figure 2 is termed the Pareto-optimal front [10,11]. This diagram, which illustrates this important tradeoff between  $J_2$  and  $J_3$  within the interval of optimality, provides new information on the dynamical interaction between the constituent cost functions ( $J_2$  and  $J_3$ ). The tangent line corresponds to  $\alpha = 1$  or  $J_2 + J_3 = \text{constant} = 2$ . For the case  $\alpha \neq 1$ , the slope of the line in Figure 2 will change accordingly and the solution can be obtained graphically. The straight line is used to equally weight the cost functions  $J_2$  and  $J_3$ , since they are initially considered to be of equal importance. The tangent line touches the curve when both the linear constraint is satisfied as well as when both cost functions are simultaneously minimized. To summarize the value added from studying the Pareto-optimal Front:

- (1) This is the region where  $J_2$  and  $J_3$  compete with one another to minimize  $J_1$ .
- (2) The constraint (e.g.  $\alpha = \text{constant}$ ) can be used to find the optimal solution.
- (3) The Pareto-optimal Front describes precisely how  $J_2$  and  $J_3$  interact with each other. The  $\alpha$  describes the degree of weighting between  $J_2$  and  $J_3$ .

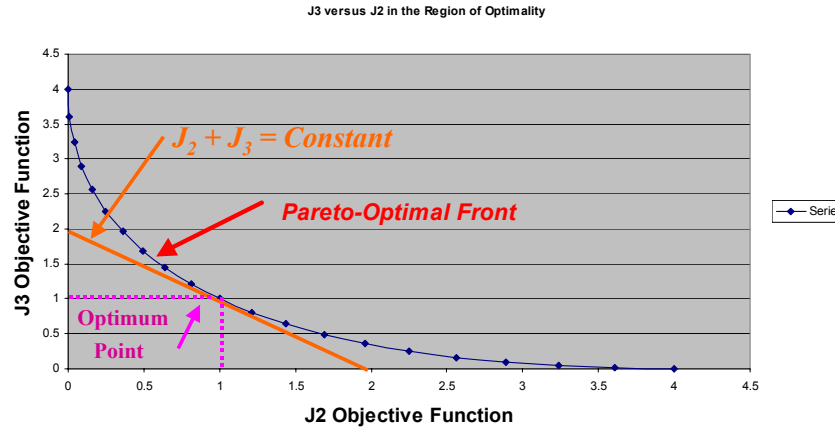


**Figure 2. Pareto-Optimal Front when plotting  $J_3$  versus  $J_2$ .**

Thus the goal is to use this technique to discover such efficiency frontiers (Pareto-optimal fronts) with humans as they perform special tracking tasks. This tells us what underlying features of human behavior occur and how the human weights certain cost functions. We now describe competing objectives of human operators that are amenable to this analysis.

### 3. COMPETING COST FUNCTIONS FOR THE HUMAN OPERATOR IN MANUAL CONTROL TASKS

In this paper we will develop a complex cost function (similar to  $J_1$ , which has constituent components  $J_2$  and  $J_3$ ), representing a tradeoff of speed and accuracy in tracking. A well-known manifestation of human tracking behavior includes the trading off of speed to accuracy as is well documented in [12-14]. Figure 3 provides a rendering of one of the most accepted mathematical models of human performance termed Fitts' Law (cf. [12] and [13] for applications). In Figure 3, a plot is made of the dependent measure (time in seconds to complete a task) versus the independent variable (bits or task difficulty). If the units of bits are used on the horizontal axis, then the resulting curve is nearly linear. The intercept point of this line with the vertical axis (labeled RT in Figure 3) occurs for a simple ballistic motor response, with essentially zero difficulty and denotes pure reaction time. The reason why this curve represents a speed-accuracy tradeoff is because for short time periods (fast responses), the accuracy or difficulty is near zero. For a much more difficult task, a slower response would occur as indicated by the slanting line to the upper right in Figure 3. Thus when speed is high, accuracy is low; when speed is low, then accuracy can be high and this inverse relationship is demonstrated. A description of the human-machine interface problem is presented next.

### 4. THE HUMAN-MACHINE INTERFACE PROBLEM

The problem of interest to be considered here is portrayed in Figure 4. The human appears in a loop with a target forcing function ( $f_t$ ). A second forcing function ( $f_d$ ) is a disturbance input. The goal of the operator in the loop is disturbance rejection of the disturbance ( $f_d$ ) forcing function, yet still keep track on the target ( $f_t$ ). Typically in applications,  $f_t$  is more of a deterministic signal (following a flight path) and  $f_d$  is more of a noisy signal (wind turbulence). This implies that the goal is to minimize the tracking error  $e(t)$  in the loop as displayed in Figure 4.

Operationally this is equivalent to maintaining a constant pose, e.g. when a helicopter is in a search and rescue mission at a low altitude and subjected to wind turbulence. The pilot, in this situation, must maintain a constant position and orientation of the aircraft subject to disturbance inputs. For this study the design parameters to be enhanced via the GA procedure are related to the spectral characteristics of  $f_t$  and  $f_d$ . Both the target and disturbance input forcing functions will be constrained to be the sum of a selected group of sine waves but characterized in a form amenable to a study involving GAs.

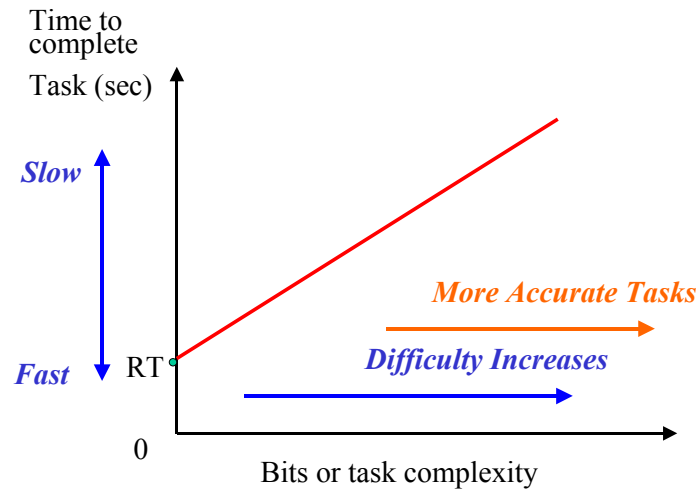


Figure 3. Fitts' Law for Speed-Accuracy Tradeoffs.

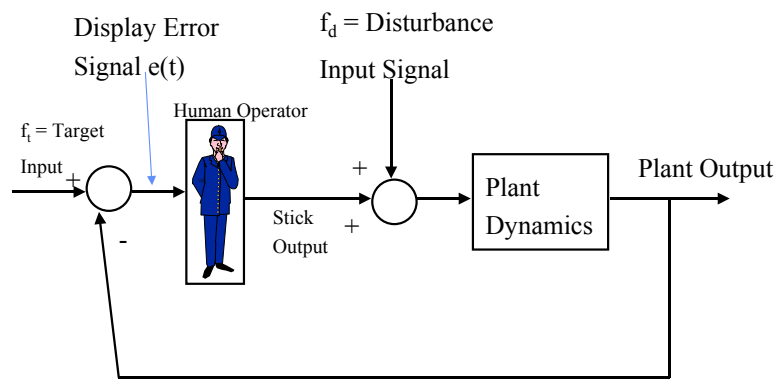


Figure 4. The Human-Machine Problem of Interest.

## 5. FORMULATION OF THE GENETIC ALGORITHM PROBLEM

The key objective in this study is to design forcing functions  $f_t$  and  $f_d$  in such a manner as to improve the human-machine interaction. The basic elements of a Genetic Algorithm problem are first discussed.

### 5.1 Development of the Basic Gene or Chromosome

Figure 5 displays an 8-bit word to describe how the GA method will be applied.

This word is a digital means of characterizing the possible candidate forcing functions  $f_t$  or  $f_d$ . Each forcing function is represented by the following series ( $i = t$  or  $d$  for target and disturbance, respectively):

$$f_i = \sum_{j=1}^8 a_j \sin(\omega_j t + \phi_j) \quad (i = t \text{ or } d) \quad (4)$$

where the eight coefficients  $a_j$  can be either high or low to be consistent with Figure 5 and  $\phi_j$  is a random phase angle. In Figure 5, the high and low representations are described by a one or zero to be viewed

# $2^8 = 256$ Possibilities

1	1	1	1	1	1	1	1
or	or	or	or	or	or	or	or
0	0	0	0	0	0	0	0

**Figure 5. The Class of Forcing Functions as An Eight Bit Word.**

within the context of an 8 bit word commonly used in computer programming. Also note that in any logical electrical circuit, the low value has a nonzero voltage component. In actuality, with equation (4) for  $f_i$ , the low value of the coefficient  $a_j$  was selected as 1.0 and the high value of  $a_j$  was selected as 2.0. Thus each forcing function was the sum of 8 sinusoids with the coefficients either 1 or 2. The bandwidth (max  $\omega_j$ ) of the forcing function  $f_i$  in equation (4) was limited to 2 Hz, since human tracking rarely is successful for frequencies beyond that range. This forcing function is actually a deterministic signal but appears quasi random to the human. For more discussion on this topic, please refer to the appendix of [15]. Figure 6 displays an FFT of the forcing function designed for the word (10000000). In the construction of the forcing function, additional steps need to be taken as follows: (1) the fundamental frequency  $\omega_0$  is defined as the reciprocal of the total task time (98 seconds) and (2) the selected frequencies  $\omega_j$  in equation (4) are prime number multiples of  $\omega_0$ . This keeps the Fourier analysis from having a foldover effect if any two  $\omega_j$  and  $\omega_k > \omega_0$  were precise integer combinations of each other and  $j \neq k$ . It is

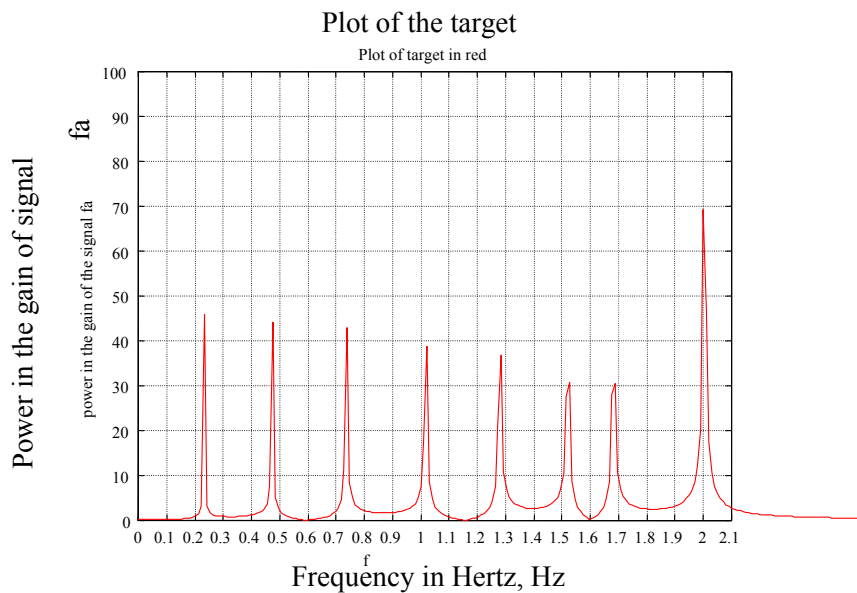


**Figure 6. Plot of the Target Forcing Function.**

also noted that the target and the disturbance forcing functions have component frequencies which have different prime number multiples of  $\omega_0$  so they could be analyzed separately and no cross correlation would exist between these variables.

### 5.2 Fitness Parameters

Three cost functions will be used to evaluate the fitness of the candidate genes during each generation of the GA search. The first fitness function is related to accuracy (minimum  $F_1$ ) of tracking. The second and third cost functions (minimum  $F_2$  and  $F_3$ ) are related to speed in acquiring a target.

This can be described more succinctly as:

$$\text{Minimize } F_1(x_1, x_2) = (T(e(t)))^2 \quad (5)$$

$$\text{Minimize } F_2(x_1, x_2) = (k_1/g_1)^2 \quad (6)$$

$$\text{Minimize } F_3(x_1, x_2) = (k_2/g_2)^2 \quad (7)$$

$$\text{Subject to: } 1 \leq x_1 \leq 256 = 2^8 \quad (8a)$$

$$1 \leq x_2 \leq 256 = 2^8 \quad (8b)$$

where  $e(t)$  is the tracking (display) error in Figure 4,  $x_1$  and  $x_2$  are the integer stick forcing function numbers. The time out of the box ( $T(e(t))$ ) is determined by the integrated time the error signal gets bigger than a threshold  $\Delta$  and can be expressed:

$$T(e(t)) = \int_0^{t_f} | [e(t') - \Delta] | dt' \quad (9)$$

where  $t_f=98$  seconds is the time duration of the tracking task. Thus if the  $T(e(t))$  variable is 9.8 seconds, this implies the error signal gets bigger than the box size  $\Delta$  for about 10% of the time during the tracking task. This is truly an accuracy measure in the sense that large deviations need to be penalized. Thus, minimizing  $F_1$  is performing an accuracy task. The terms  $g_1$  and  $g_2$  in equations (6,7) are speed measures (bandwidth), as described in the appendix. Hence, minimizing  $F_2$  and  $F_3$  (increases bandwidth and speed) and trades off against  $F_1$ . The best forcing function set,  $\{x_{1best}, x_{2best}\}$ , defines the best combination of forcing functions to achieve preferred operator performance.

To recapitulate the procedure so far, the selection is made of  $J_4$  the overall cost function to minimize defined via:

$$J_4 = F_1 + F_2 + F_3 \quad (10)$$

$$\text{or } J_4 = (T(e(t)))^2 + (k_1/g_1)^2 + (k_2/g_2)^2 \quad (11)$$

which will lead to a Pareto-optimal front since  $F_1$  is known to trade off with either  $F_2$  or  $F_3$ , from prior studies in this area.

From a performance perspective and akin to the prior discussion on Pareto-optimal fronts, there has been an extensive past history in modeling human behavior via cost functions that have competing constituent components. For example, Elkin et al. [23] and Barron et al. [24] looked at ways humans trade off control effort to tracking accuracy. The equivalence between control effort and bandwidth in the human-machine literature is also a common assumption [25].

The remaining relevant issues regarding the GA study are now described.

### 5.3 Evaluating Genes

Following accepted procedures [16], the two 8-bit chromosomes (characterizing  $f_t$  and  $f_d$ ) were randomly initialized and the fitness function calculated.

### 5.3.1 Fitness Allocation

The use of genetic algorithms for multi-objective optimization is not new (see [16] for a review). Of the variation between existing techniques, much can be attributed to the method of allocating fitness that reflects proximity to the Pareto-optimal frontier. While several techniques show promise, no single genetics-based multi-objective optimization method has demonstrated a clear superiority over the others. For the current problem, we selected the non-dominated sorting GA, or NSGA, as our baseline. NSGA is a fitness assignment algorithm originally based on Goldberg's ideas [17] and first implemented in [18]. In NSGA, the fitness assignment algorithm favors non-dominated solutions and uses a sharing strategy to preserve diversity among solutions of each non-dominated front.

The NSGA algorithm is described in the following steps:

Step 1: Select a sharing parameter,  $\sigma_s$ , and a gap parameter,  $\varepsilon$ , to distinguish between elements of different Pareto-optimal frontiers.

Step 2: Sort the population according to non-domination. This step results in a stratification of frontiers so that the first frontier contains the set of non-dominated solutions, the second frontier contains a set of solutions dominated only by the first set, and successive frontiers that are only dominated by solutions contained in previous frontiers.

Step 3: For each frontier,  $i$ , of non-dominated solutions, set the maximum fitness function as

$$F_i = F_{i-1} - \varepsilon \quad (12)$$

Within each frontier, we calculate the fitness value of each candidate solution,  $j$ , as

$$F_i^j = F_i / nc_j \quad (13)$$

Where the niche count of  $j$ , denoted as  $nc_j$ , is defined as,

$$nc_j = \sum_{k=1}^n sh(d_{jk}), \quad (14)$$

where  $n$  is the number of candidate solutions in frontier  $i$  and  $sh(d_{jk})$  is a sharing function that measures the dispersion between candidate solutions  $j$  and  $k$ . The sharing function is defined as:

$$sh(d_{jk}) = \begin{cases} 1 - \left( \frac{d_{jk}}{\sigma_s} \right), & \text{if } d_{jk} \leq \sigma_s; \\ 0, & \text{otherwise.} \end{cases} \quad (15)$$

where  $d_{jk}$  is the normalized Euclidean distance which is defined as,

$$d_{jk} = \sqrt{\sum_{l=1}^m \left( \frac{x_l^j - x_l^k}{x_l^{\max} - x_l^{\min}} \right)^2} \quad (16)$$

where  $x^j$  and  $x^k$  are decision variables. The NSGA algorithm results in a ordering of candidate solutions so that those along the non-dominated frontier are ranked higher than those in dominated frontiers. Moreover, within each frontier, decision variables that are not clustered together are ranked higher than those that are.

Once the fitness values for each chromosome are assigned, standard GA selection, crossover, and mutation operators are then applied.

### 5.3.2 Selection

There exist numerous selection techniques in the GA literature. The Stochastic Universal Sampling (SUS) technique proposed by Baker [19] was used because it has been demonstrated as a superior method [20]. In SUS, a conceptual roulette circle is loaded with the relative fitness's of all chromosomes in the population. Attached to this circle is an equally spaced multi-armed spinner. Spinning the wheel then simultaneously selects all chromosomes for the next generation.

### 5.3.3 Crossover and Mutation

There also exist several techniques to exchange information between two chromosomes. The primary distinction between the techniques lies in the number of cut-points (i.e., locations between which information is swapped) utilized. In the case of one-point crossover, one cut-point is randomly selected and the information after that point is exchanged between two chromosomes. In uniform crossover, a predetermined probability (usually 0.5) is used to select positions where bit-wise information between two chromosomes is exchanged.

Spears [21] conducted a series of analyses on n-point recombination techniques and found that disruption to the schemata increases as n increases. Therefore, uniform crossover with a probability of 0.5 presents the most disruptive crossover technique to the preservation of schemata. However, Spears also suggests another way of interpreting the effects of uniform crossover. Not only does uniform crossover disrupt existing schemata, it also creates new building blocks. For the current problem, we have chosen the uniform crossover method. While the selection of a crossover method is not trivial, it is more important in the case of a small population (relative to the entire space of possible solutions) to generate novel building blocks than to preserve existing ones.

In [21], an extensive analysis of the mutation operator was conducted. However, because we are more concerned with the use of the crossover operator to search, we limit the role of mutation to maintain diversity. Therefore, we used a standard mutation operator to select chromosomes to mutate based on a fixed probability. Within selected chromosomes, we randomly alter the information contained in one gene.

### 5.3.4 Algorithm Execution and Results

The following settings have been recommended by [16, 22] and have been empirically determined as useful:

- Population size = 100;
- Crossover rate = 0.8;
- Uniform crossover probability = 0.5;
- Mutation rate = 0.001;
- Sharing parameter = 0.1;
- Gap parameters = 5.0
- Stopping condition = 500 generations

Five initial populations were randomly generated to assess sensitivity to initial conditions. We ran each population for 500 generations and used the data from the final generation to extract the Pareto-optimal frontier for  $F_1$  and  $F_2$ . To indicate the amount of learning accomplished the genetic algorithm on each population, we use the average distance of the population from the origin for each training generation

where 
$$\text{Average Distance} = \frac{\sum_{i=1}^{100} \sqrt{F_{1i}^2 + F_{2i}^2}}{100}$$
 and  $F_{1i}$  and  $F_{2i}$  are the objective function values

corresponding to the  $i^{\text{th}}$  chromosome in the population. Therefore, populations with average distance that are closer to the origin are better than populations that are farther away. For illustrative purposes, figures 7-10 portray the average distance of four of the five populations.

These figures exemplify GA learning for the entire population. The initial average distance ranged from 276.6 (population 4) to 285.5 (population 5) and the trained average distance for all populations was approximately 195.

By visual inspection, there appears little difference between the trained populations in terms of average distance. To confirm this suspicion, we conducted a two-way (training X population) analysis of variance (ANOVA) on the final 300 training generations. Because the intent of the analysis is to determine whether the GA is sensitive to initial conditions, we needed to factor out the variability inherent in the randomized pre-trained populations. Therefore, the first 200 generations were removed from consideration. The results of the ANOVA are provided in Table I.

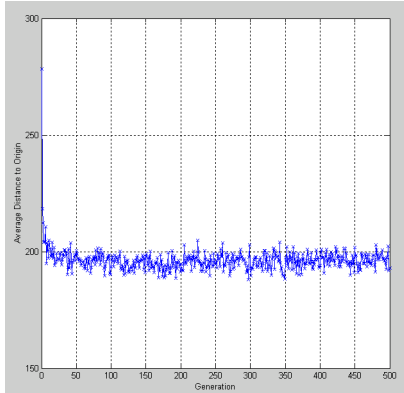


Figure 7. Population 1 Average Distance to Origin for Each Generation

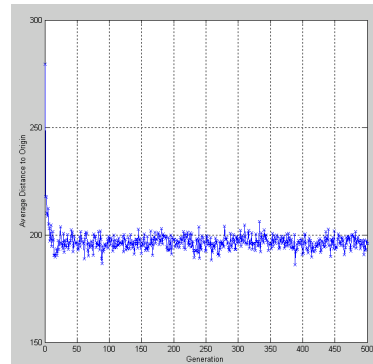


Figure 8. Population 2 Average Distance to Origin for Each Generation

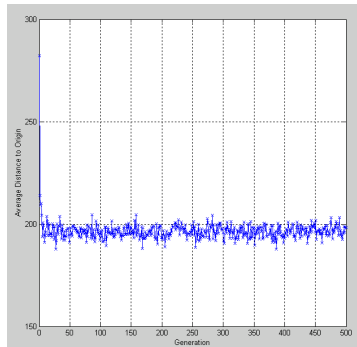


Figure 9. Population 3 Average Distance to Origin for Each Generation

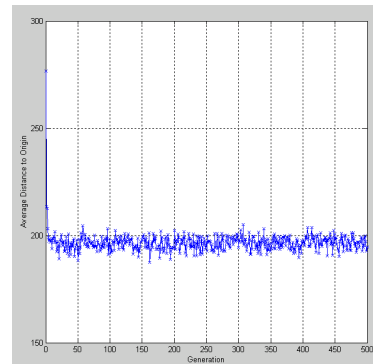


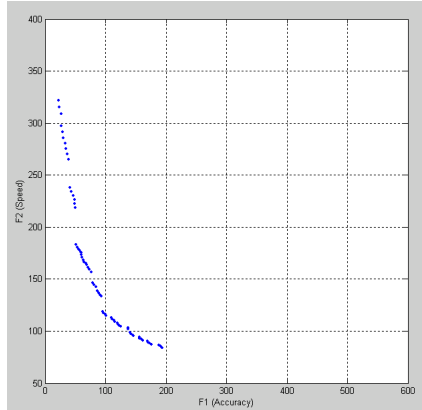
Figure 10. Population 4 Average Distance to Origin for Each Generation

Table I. Analysis of Variance for GA Training.					
	Df Effect	MS Effect	Df Error	MS Error	F
Training	5	23.79298	1470	8.586998	2.770815*
Population	4	10.00332	1470	8.586998	1.164938
Interaction	20	12.14559	1470	8.586998	1.414416

\*  $p < 0.05$

It is interesting to note that while a significant training effect ( $p < 0.05$ ) still exists, there does not appear to be a significant difference between the populations (no significant interaction). The results suggest that our GA is, for the present analysis, is insensitive to initial conditions.

The Pareto-optimal front of the trained populations is shown Figure 11. When compared with all the points sampled by the crossover procedure, it is evident that the GA captured the outlines of the ridge that represents the Pareto-optimum front.



**Figure 11. F1 and F2 Values Along the Pareto-optimal Front.**

Figure 11 may be compared with Figure 2, which involved tradeoffs for quadratic criteria. The similarity of the shapes between the two figures indicates that humans may also implicitly trade off these speed-accuracy objective functions in a quadratic manner.

Finally the experimental design scenario is described which provides the necessary experimental platform to truly show the efficacy of the proposed methodology.

## 6. EXPERIMENTAL DESIGN CONDITIONS

A brief description of the key experimental variables is presented.

### 6.1 Subjects

A total of seven subjects participated in this experiment. A subject panel from a local contractor at the Wright-Patterson Air Force Base in Ohio, USA provided

five of the participants. These adult people were either housewives or students at a local university being employed part time. The compensation for partaking in this experiment was about \$6 dollars (US) an hour for their participation. The remaining three subjects were a contractor and US Government personnel. Table II describes the demographics of the subjects used in this study.

**Table II. Demographics of the Subjects Used in the Study**

Gender – Male or Female	Age in Years	Title
Female	23	Graduate Student
Female	20	Undergraduate Student
Female	20	Undergraduate Student
Female	19	Undergraduate Student
Male	57	Research Scientist
Male	45	Computer Programmer
Male	36	Postdoctoral Associate

Figures 12a-b illustrates the chair motion simulator (for  $f_d$ ) and haptic stick (for  $f_t$  on the display) used in this experiment.

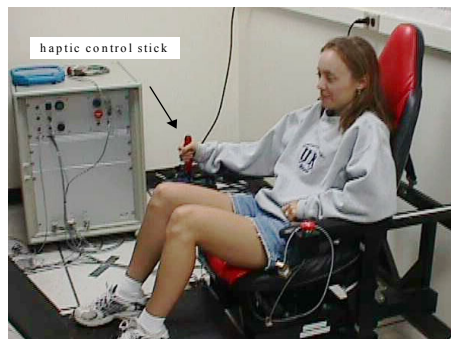


Figure 5a. Motion Base Simulator used in Pilot Study



Figure 5b. Proximal Distance from the Base to the Tracking Display

**Figures 12a-b. Experimental Apparatus to Evaluate Interface.**

## 6.2 Apparatus

This single-axis motion platform was outfitted with a dual axis force reflecting joystick controller (Immersion 2000) as displayed in Figures 12a-b. This device was constructed from a welded aluminum frame rigidly supporting a racing car seat. Padded armrests are configured at an elbow level, while the joystick is mounted such that its handle may be comfortably grasped by a seated subject's right hand. Joystick motion was restricted to the lateral axis, the axis parallel to the motion of the chair. The entire frame translates sideways on a Ball Screw assembly with an 18-inch stroke. Translation is driven by a Kollmorgen Model B-404-B DC Servo Motor, which is rated at 4.5 hp.

The Immersion IE (Impulse Engine)-2000 powered joystick is a two-degree of freedom force-reflecting manipulandum used in haptic experiments. It generates about 4.04 Newton's maximum force at the handle grip to the human operator, which is displaced 0.1397 meters from a pivot point. This device measures position displacement of the stick through digital encoders and applies a force feedback interface via a cable drive. The force reflection algorithms are programmable in C++ code. The forces generated by this haptic device are independent of the chair's motion but the chair may induce a physical interaction upon the human operator to generate biodynamic feed through at the joystick.

## 6.3 The Performance Task and Performance Measures

As discussed earlier, the subject was instructed to keep the cross cursor within the box as much as possible. This task was exposed to disturbances affecting the cross and the chair motion which was inducing a biodynamic feed through effect by moving the arm of the subject. The experimental validation of this study was conducted in two parts. Part 1 was the pilot study to build a computer model to be tested by the GA methodology. Next, the enhanced design parameters were selected. Finally, the Part 2 study involved seven subjects in a post-hoc experimental validation of the enhanced design parameters selected via the GA algorithm. The subjects were presented the experimental conditions in random order based on a simple Latin Square design commonly used in experimental studies.

## 6.4 The Pilot Study – Part 1

Figure 13 illustrates the 4x4 matrix of experimental design conditions ( $f_t$  and  $f_d$ ) used to span the space of candidate forcing functions ( $f_t$  and  $f_d$ ) and to help develop a preliminary model of the human-machine interaction. These conditions were presented randomly to the subjects in the pilot study with four data days for each subject.

## 7. MODELING THE HUMAN-MACHINE INTERACTION

A simple, parsimonious model to characterize human-machine interaction is selected to assist in this process.

### 7.1 The Crossover Model of Human Tracking Performance

The appendix describes the "Crossover Model" [14], which has been widely used in the literature to describe human-machine interaction. This simple, parsimonious model was appropriate to simplify key attributes of the human-machine interaction.

### 7.2 The Basic Model Derived From the Part 1 – Pilot Study

The equations for  $g_1$  and  $g_2$  previously described in (6,7) were obtained from the pilot study for the forcing functions in the range  $x_1 \in [1, 256]$  and  $x_2 \in [1, 256]$ . For example, the bandwidth term  $g_1$ , (estimate of  $\omega_c$ ) the model can be displayed as follows:

$$g_1(f_t, f_d) = 112.5 + (30/155)*x_1 + (40/98)*x_2 \quad \text{for } (x_1 \in [1,128], x_2 \in [1,128]) \quad (17)$$

$$g_1(f_t, f_d) = 203 - (33.5/155)*x_1 - (40/98)*x_2 \quad \text{for } (x_1 \in [129,256], x_2 \in [129,256]) \quad (18)$$

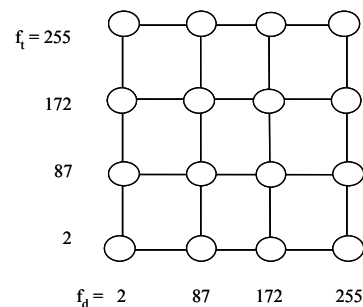


**Figure 13. Pairs of Target and Disturbance Forcing Functions Used in Pilot Study.**

### 7.3 The Simulink Simulation

Figure 14 portrays the Simulink Simulation, which was run  $2^{16}$  times in a search for enhanced design parameters. In this diagram both  $f_t$  and  $f_d$  enter into a real time simulation. The  $g_1(\cdot)$  and  $g_2(\cdot)$  terms are calculated similar to equations (17-18) and the  $T(e(t))$  value was determined through the computer simulation. With this additional information, the objective functions  $F_1$ ,  $F_2$  and  $F_3$  can then be evaluated for all  $2^{16}$  possible experimental design conditions. From this computer simulation, a response surface is then determined.

### 7.3 The Response Surface to be Searched

Figure 15 illustrates the response surface to be searched after the model in Figure 14 was run for all possible ( $2^{16}$ ) candidate  $f_t$  and  $f_d$  design parameters.

In the above diagram, the response surface is displayed, for simplicity, as a scalar cost function  $J_4 = F_1 + F_2 + F_3$  to show the nonconvex nature of this model interaction. The minimum of  $J_4$  represents the ideal operating point, which was also found by the vector process Pareto-optimal front. This minimum is a consequence of a human having a finite speed and accuracy in the best operation conditions of this experiment. The final step in this process is to take the best choices of  $f_t$  and  $f_d$  and to evaluate them in a post-hoc experimental test to demonstrate the efficacy of this proposed method.

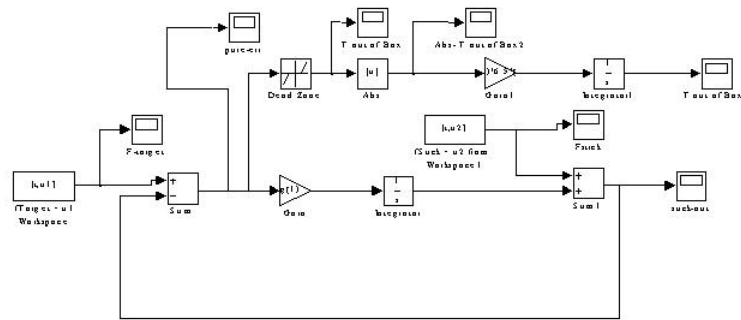


Figure 14. SIMULINK Diagram to Emulate Human-Machine System

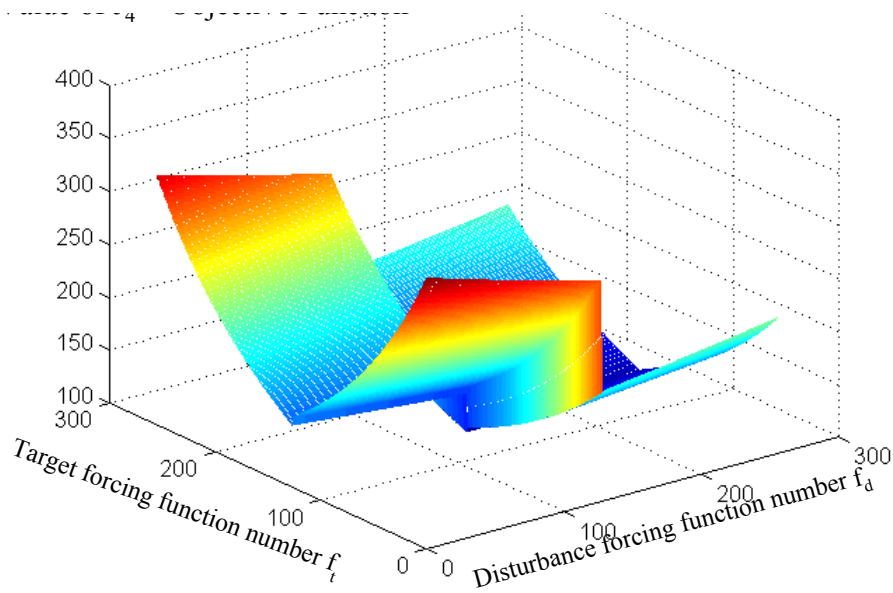


Figure 15. Plot  $J_4$  versus  $f_t$  and  $f_d$  – all 256x256 cases Value of  $J_4$  = Objective Function.

Three important reasons are now given why the set of 256x256 forcing functions were chosen as the granularity size to explore this sensory input. The reasons include: (a) Runs with human subjects could not exceed 2 minutes in duration which limited the fundamental frequency, (b) The interweaved frequencies had to be prime number multiples of the fundamental frequency as well as being different from each other, and (c) The computer simulation described in Figure (15) took about 60 hours of real time on a personal computer for  $2^{16}$  possibilities of the forcing function combinations. If this granularity were to be increased, the computation time to produce Figure (15) may be outside the range of practicality. The reason why Figure (15) took so long to generate was that it included a hybrid simulation in both SIMULINK™ and MATLAB™. The combined MATLAB-SIMULINK™ system running time took about 30 seconds to initialize between both computer programs, run the simulation in SIMULINK™, and store the results for each loop iteration. Also, please note that the GA study employed 500 generations of 100 individuals for a total of 50,000 runs. This number is still less than the  $2^{16}$  size of the landscape of the fitness function  $J_4$  selected for this study.

## 8. THE PART II -VALIDATION STUDY

In this Part II validation, seven subjects were run at the best design conditions ( $x_1 = f_{t \text{ best}}^*$  and  $x_2 = f_{d \text{ best}}^*$ ) versus alternative selected conditions. The best design conditions were determined from the minimum of the response surface in Figure 15 which was also determined from the Pareto-optimal front analysis previously discussed. Figure 16 shows this experimental design matrix selected to evaluate the subjects at the enhanced condition versus alternative conditions. As stated in section 2, the subjects were presented the experimental conditions in random order based on a simple Latin Square design commonly used in experimental studies. Four replications of each of the conditions illustrated in Figure (16) were conducted.

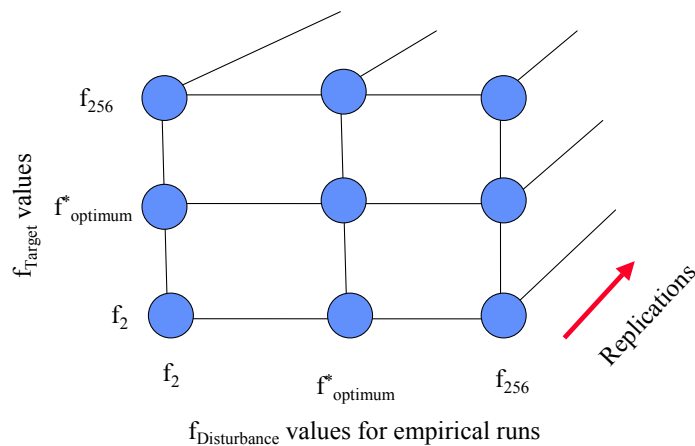


Figure 16. Post Hoc Experimental Design Matrix for Validation

### 8.1 Statistical Testing of the Enhanced Design

#### 8.2 Hypothesis/Objectives

In the null hypothesis, it is desired to reject that the enhanced design of selective parameters from the GA search did not improve measures of human performance in a post hoc evaluation with human subjects. For simplicity, performance will be measured by the scalar  $J_4$  value defined earlier. That is, the null hypothesis is given by:

$H_0$ : There is no difference in empirically determined  $J_4$  due to the use of ( $f_{t \text{ best}}^*$  and  $f_{d \text{ best}}^*$ ) as compared to alternative experimental conditions.

## 9. RESULTS

Seven subjects were run via the experimental design conditions as depicted in figure 16. To conduct an analysis of variance, the  $J_4$  ( $J_4 = F_1 + F_2 + F_3$  from equations (5-7)) function was evaluated empirically as a dependent scalar measure to reflect the performance of the final design. Table III illustrates the mean and standard deviations of the  $J_4$  variable obtained from this post-hoc experimental study (cf. Figure 17).

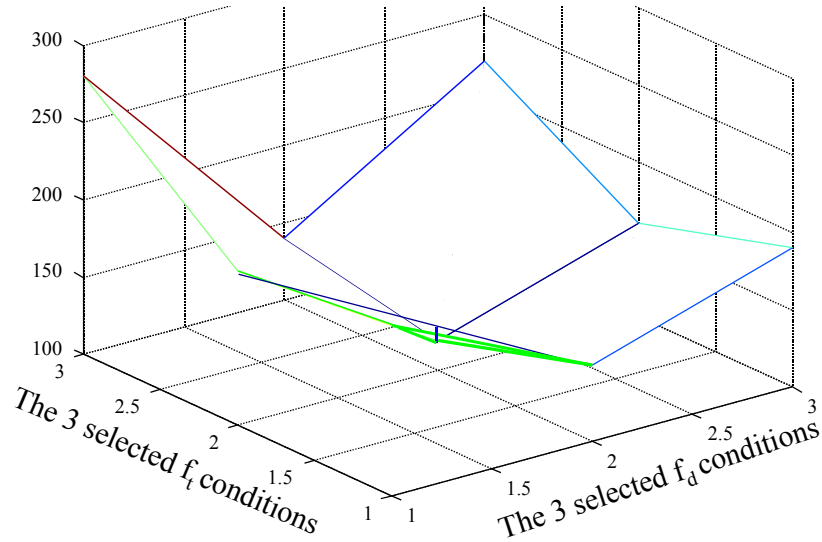


**Figure 17. Post Hoc Analysis of  $f_t$  and  $f_d$  with Human Subjects Empirical  $J_4$  Values.**

From Table IV, we see that it is possible to significantly ( $p < .05$ ) reject the null hypothesis that the best condition ( $f_{t\text{-best}}$ ,  $f_{d\text{-best}}$ ) was no different from the alternative conditions as portrayed in Figure 17. From the means of the  $J_4$  values in Table III, it is obvious that  $J_4$  is much reduced at the best conditions ( $f_{t\text{-best}}$ ,  $f_{d\text{-best}}$ ) versus the alternative choices. Thus the human-machine interface has been designed in an enhanced sense for diminished values of  $J_4$ , which are related to both increased accuracy and performance tracking capability. Also, in Table IV, the interaction term is not significant ( $p=0.3088$ ) for the choice of these independent variables. This confirms the earlier assumption on the construction of the candidate forcing functions ( $f_t$  and  $f_d$ ) was such that they would not interact with each other by the performance measure ( $J_4$ ) selected to be improved. Finally, it is noted that  $J_4 > 0$  cannot be zero because of the conflicting requirements specified by equation (11) as well as the fact that the performance task was chosen to be sufficiently difficult that some tracking error would result.

**Table III. Mean and Standard Deviation values of  $J_4$  Across Seven Subjects.**

Target $f_t = f_t$	Disturbance $f_d = f_d$	Mean of $J_4$	S.D. of $J_4$
f-2	f-2	222.5023	54.71826
f-2	f-opt	177.6658	31.87641
f-2	f-256	186.5249	37.16178
f-opt	f-2	204.3841	23.71543
f-opt	f-opt	131.5212	27.51218
f-opt	f-256	186.0831	35.85972
f-256	f-2	254.2873	26.6152
f-256	f-opt	160.1628	32.85745
f-256	f-256	213.1491	22.69241

**Table IV. Results of ANOVA Across Seven Subjects in Post Hoc Study.**

Factor	Degrees of Freedom	Sum of Squares	F-Ratio	Prob > F
f- Target = $f_t$	2	13612.4	6.1354	.0040
f-Disturbance = $f_d$	2	58664.5	26.4414	<.0001
f-Target * f-disturbance	4	5460.6	1.2306	0.3088

An analysis of variance (ANOVA) was then conducted with the data summarized in Table III. The results of the within subjects ANOVA are displayed in Table IV.

## 10. CONCLUSIONS

A GA method was utilized to search a large space of possible experimental design parameters in conceiving how haptic devices impact human tracking performance and speed characteristics in tracking. A preliminary model was developed using pilot data. A computer simulation was then conducted  $2^{16}$  times with this preliminary model to predict enhanced or best experimental design conditions. In a post hoc study with seven human subjects, the enhanced experimental design conditions were compared to alternative conditions to demonstrate the efficacy of the proposed method. The limitations of this approach are predicated on the granularity of the number of forcing functions chosen (256 for each independent variable in this paper) as to the resolution of the process. In addition, a larger number of subjects would always add credence on the procedure. Since one of the goals was to develop a parsimonious model to help predict data in a more expanded setting, this objective was demonstrated in the post hoc study. Future research will expand both the number of subjects and with improved granularity (increasing numbers of forcing functions) for each of the independent variables of interest to better refine this model.

## REFERENCES

- [1] T. L. Chelette, D. W. Repperger and C. A. Phillips, 1996. Pattern Recognition of Spastic Motion, *Journal of Intelligent & Fuzzy Systems*, **4**, 141-160.
- [2] C. D. Stylios and P. P. Groumpos, 2000. Fuzzy Cognitive Maps in Modeling Supervisory Control Systems, *Journal of Intelligent & Fuzzy Systems*, **8**, 83-98.
- [3] M. A. Jarrah and A. Shaout, 2001. Fuzzy Modular Autonomous Intelligent Cruise Control (AICC) System, *Journal of Intelligent & Fuzzy Systems*, **11**, 121-134.
- [4] A. Pouliezios, D. Papadimitriou and G. Tselentis, 2000. Fuzzy vs. 'Manual' Control in a FeNi Plant, *Journal of Intelligent & Fuzzy Systems*, **8**, 229-242.
- [5] K. Z. Tang, K. K. Tan, C. W. de Silva, T. H. Lee and A. S. J. Chin, 2001. Monitoring and Suppression of Vibration in Precision Machines, *Journal of Intelligent & Fuzzy Systems*, **11**, 33-52.
- [6] T. Senjyu, A. Miyazato and K. Uezato, 2000. Enhancement of Transient Stability of Multi-Machine Power Systems by Using Fuzzy-Genetic Controller, *Journal of Intelligent & Fuzzy Systems*, **8**, 19-26.
- [7] T. Sawaragi, N. Tani, and O. Katai, 1999. Evolutional Concept Learning from Observations through Adaptive Feature Selection and GA-Based Feature Discovery, *Journal of Intelligent & Fuzzy Systems*, **7**, 239-256.
- [8] H. Ding and Madan M. Gupta, 1997. Learning Fuzzy Set Neural Networks by Genetic Algorithms, *Journal of Intelligent & Fuzzy Systems*, **5**, 113-127.
- [9] T. Samatsu, E. Uchino and T. Yamakawa, 2000. Feature Extraction of a Vectorcardiogram by Employing a Wavelet Network Guaranteeing a Global Minimum, *Journal of Intelligent & Fuzzy Systems*, **8**, 221-227.
- [10] V. Pareto, 1986. *Cours d' Economie Politique*, Rouge, Lausanne, Switzerland.
- [11] Schaffer, 1985. Multiple Objective Optimization with Vector Evaluated Genetic Algorithms, *Proceedings of the First International Conference on Genetic Algorithms and Their Applications*.
- [12] P. M. Fitts, The Information Capacity of the Human Motor System in Controlling the Amplitude of Movement, *Journal of Experimental Psychology*, **47**, pp. 381-391.

- [13] D. W. Repperger, C.A. Phillips and T. Chelette, 1995. Study of Spatially Induced ‘Virtual Force’ With An Information Theoretic Investigation of Human Performance, *IEEE Transactions on Systems, Man, and Cybernetics*, **25** (10), pp. 1392-1404.
- [14] D. McRuer, et al., 1967. Manual Control of Single Loop Systems- Parts I and II, *J. Franklin Institute*, **283** (1 and 2).
- [15] D. W. Repperger and D. B. Rogers, 1983. Behavioral Modeling: Validation and Information Theory Considerations, *Mathematical Modeling*, **4**, pp. 209-222.
- [16] Deb, K. 2001. *Multi-Objective Optimization using Evolutionary Algorithms*. New York: John Wiley & Sons, Ltd.
- [17] D. E. Goldberg, 1989. *Genetic Algorithms in Search, Optimization, and Machine Learning*. New York: Addison-Wesley Publishing.
- [18] Srinivas, N. and Deb, K. 1994. Multi-objective Function Optimization Using Non-dominated Sorting Genetic Algorithms. *Evolutionary Computation Journal*- **2** (3), 221-248.
- [19] Baker, J.E. 1987. Reducing Bias and Inefficiency in the Selection Algorithm. In J.J. Grefenstette (Ed.), *Proceedings of the Second International Conference on Genetic Algorithms* (14-21). Cambridge, MA.
- [20] Reeves, C.R. 1997. Genetic Algorithms for the Operations Researcher. *INFORMS Journal on Computing*- **9** (3), 231-250.
- [21] Spears, W.M. 1998. *The Role of Mutation and Recombination in Evolutionary Algorithms*. Ph.D. dissertation, Department of Computer Science, George Mason University.
- [22] Mitchell, M. 1996. *An Introduction to Genetic Algorithms*. Cambridge, MA: The MIT Press.
- [23] Elkind, J. I., Falb, P., Kleinman, D. L., and Levison, W. H., 1968, An Optimal Control Model for Predicting Control Characteristics and Display Requirements of Manual Vehicle Systems, TR-AFFDL-67-187, US Air Force.
- [24] Baron, S. and Kleinman, D. L., 1969, The Human as an Optimal Controller and Information Processor, *IEEE Trans. on Man-Machine Systems*, **MSS-10**, (1), pp. 9-17.
- [25] Sheridan, T. B. and Ferrell, W. R., 1981. *Man-Machine Systems – Information, Control, and Decision Models of Human Performance*, The MIT Press.

## ABOUT THE AUTHORS



D. W. Repperger received his BSEE and MSEE degrees from Rensselaer Polytechnic Institute and his PhD in Electrical Engineering from Purdue University. His research interests include computational algorithms and human-machine systems. Presently he is at the Air Force Research Laboratory, Wright-Patterson AFB in Ohio, USA.

L. Rothrock received his doctorate in Industrial Engineering from the Georgia Institute of Technology and is currently an Assistant Professor in the Department of Industrial and Manufacturing Engineering at Pennsylvania State University. Dr. Rothrock’s research areas include human-in-the-loop simulations, display visualization, and human-machine performance assessment.



## APPENDIX - THE CROSSOVER MODEL OF HUMAN TRACKING PERFORMANCE

A classical model of human-machine interaction is the “Crossover Model” (McRuer et al., [14]), which has been widely used in the literature to describe human-machine interaction. The simplicity and parsimonious nature of the model have made it an attractive means of describing human behavior in a manner that is easily understood.

Figure A.1 describes a simplification of the human-machine system into a block diagram form using the Crossover Model Assumption. The parameter  $\omega_c$  is the crossover frequency and represents an approximate measure of the bandwidth of the closed loop system between  $f_t$  and the plant output variable.

The  $s$  variable is the Laplace transform and the presumption is that the time delay  $\tau$  is relatively small for this study. The plant dynamics are unity in this analysis so that the variable  $f_d$  can be assumed to appear at the plant’s output. The focus of this study will be on the optimal design of the two key parameters  $f_t$  and  $f_d$  to optimize a multi-objective function related to human tracking performance.

By taking the closed loop transfer function (assuming  $\tau \approx 0$ ) of the system in Figure A.1, the loop gain which relates how the Plant Output depends on both  $f_t$  and  $f_d$  can be specified as follows.

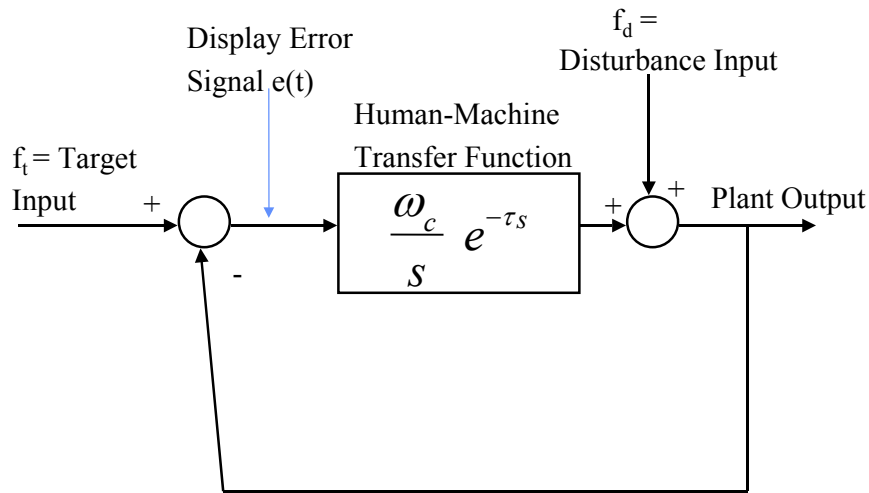


Figure A.1. The Crossover Model of Human-Machine Interaction.

$$\text{Loop Gain} = \frac{\frac{\omega_c}{s}}{1 + \frac{\omega_c}{s}} = \frac{\omega_c}{s + \omega_c} \quad (\text{A.1})$$

Viewing equation (A.1) in terms of a low pass filter, the bandwidth of the closed loop system is proportional to  $\omega_c$ . Thus, speed is proportional to  $\omega_c$ . In equations (6,7), the terms  $g_1$  and  $g_2$  are estimates of  $\omega_c$  empirically determined by fitting a low pass filter to spectral analysis of the closed loop transfer function and estimating the crossover frequency ( $\omega_c$ ) via this procedure. Mean values of  $g_1$  and  $g_2$  were slightly different from one another in the calculation of the closed loop bandwidth (estimate of ( $\omega_c$ )).